# A 2-Way Daly-Type Beam Diagnostic System for TITAN EBIT

By

Cecilia Leung

TRIUMF Undergraduate Summer Student

Faculty of Science and Engineering
Department of Physics and Astronomy
York University

August 2007

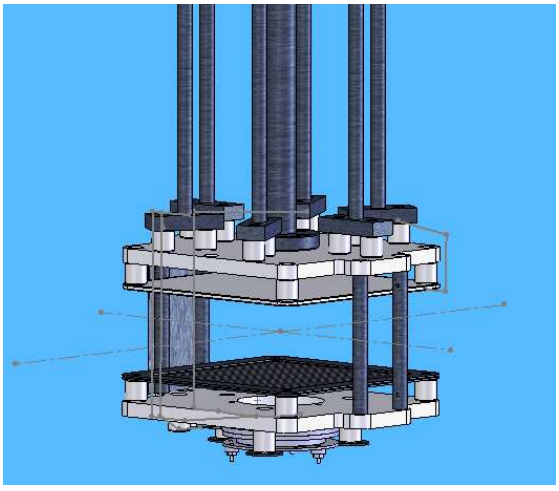

# CONTENTS

# ABSTRACT

A Daly-type diagnostic system was developed for the TRIUMF TITAN experiment to detect low-intensity ion beams based on imaging secondary electrons released upon radioactive ions striking an overhanging aluminum plate. The system provides on-line information about the intensity and spatial distribution of the beam and is effective for alignment and imaging purposes. In addition, the design enables the reception of beam from either ends of the structure and thus satisfies the condition of a 2-way detection system.


# 1 INTRODUCTION

## 1.1 TRIUMF

TRIUMF, TRI-University Meson Facility, is Canada's National Laboratory for Particle and Nuclear physics. It is a world-class subatomic physics research laboratory located on the campus of the University of British Columbia in Vancouver, Canada. TRIUMF is operated by a consortium of 13 Canadian member and associate member universities and is publicly funded by the federal government through the contribution of the National Research Council of Canada.

Fig. 1 The TRIUMF facilities on the campus of the University of British Columbia

At the heart of the facility lies the world's largest cyclotron. At 18m in diameter with a main magnet weighing 4000 tonne, it is used to accelerate 100 trillion protons up to energies of 500 MeV every second. Hence, TRIUMF produces one of the most intense proton beams in the world. By making these protons strike different kinds of targets, high-intensity beams of neutrons, pions, muons, as well as exotic isotopes can also be created. The research conducted at TRIUMF ranges from particle physics, nuclear physics, and astrophysics, to practical application in fields such as material sciences and medical therapy.

## 1.2 ISAC

The two ISAC, Isotope Separator Accelerator, facilities have greatly expanded the possibilities for leading edge experimentation at TRIUMF at a time when research with radioactive beams are gaining increasing importance in nuclear physics.

Beams of short-lived radioactive isotopes can be created by bombarding a suitable solid target with high-intensity protons from the main cyclotron. TISOL (TRIUMF Isotope Separator On-Line) allows for the separation of the desired radioisotopes from others that may be formed simultaneously and a linear accelerator speeds up these short-lived radioactive particle/isotopes beams to much higher velocities before delivering them to various experiments.

The ISAC facilities enable us to simulate and understand the nuclear reactions which occur during stellar explosions so that we may study the properties and structure of these exotic isotopes along with their process of nucleosynthesis. In addition, by studying the properties of nuclei which are far from the line of stability scientists can explore the limits and tests the predictions of the Standard Model in an attempt to provide us with a clearer picture of the ultimate basis of all matter.

## 1.3 TITAN

The primary goal of TITAN, TRIUMF's Ion Trap for Atomic & Nuclear physics, is to performs high-precision ($\delta m/m \leq 10^{-8}$) atomic mass measurements on short-lived ($t_{1/2} \geq$ 50ms) isotopic radionuclide to test the predictions of the Standard Model, and models of the nuclear-structure and nuclear astrophysics.

The atomic mass, related to the binding energy, is a fundamental property of nuclei determined by the sum of the masses of the individual protons and neutrons minus the mass equivalent of their binding energy. By adding one neutron at a time and measuring the changes in binding energy, we can start to map out and understand in a controlled and systematic way where the limits of how many nucleons can be added to the nucleus and what causes these limits. ISAC's TITAN facility, now in the bridge between the final phase of construction and the beginning of its commission, is designed to do just this.

Fig. 2 TITAN platform in the ISAC I experimental hall

Consider a highly charged ion with low energy that moves in a strong magnetic field. Experimental measurements developed at ISOLTRAP at CERN [1] determined that the ion will have a cyclotron motion with cyclotron frequency:

$$\omega_c = \frac{1}{2\pi}\frac{q}{m}B$$

So knowing the ion's charge q, magnetic field strength B, and measuring ion cyclotron frequencies, we can determine the mass.

Moreover, the precision of the mass measurement is determined by:

$$\frac{\delta m}{m} \propto \frac{m}{T_{obs} q B \sqrt{N}}$$

where m = mass of ion
t = observational time
q = ion's charge
B = applied magnetic field
N = # of ions

Since the TITAN project aims to measure the masses of short lived radioactive nuclei, it is obvious that storing such ions for long periods of time would be impossible. However, the accuracy of mass measurements in a Penning trap is also directly proportional to an ion's charge state. Hence statistical uncertainties may be reduced by injecting highly charged ions into the trap [11].

TITAN's unique combination of an RFQ, EBIT and precision Penning trap will allow radioactive isotopes with short half lives to be studied and allow mass measurements with high resolution/accuracies. The entire process of cooling, charge-breeding and trapping radioactive isotopes are produced at ISAC occurs in approximately 10 milliseconds [11].

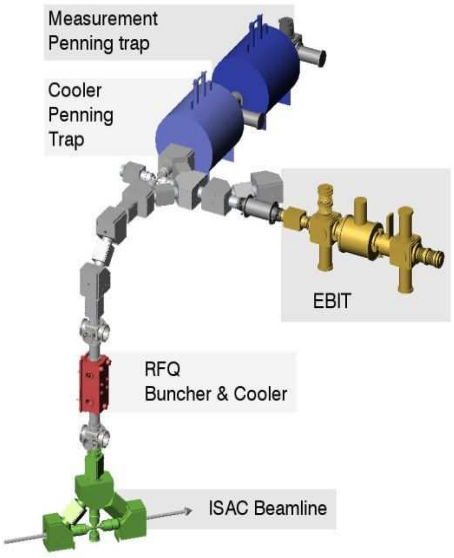


Fig. 3 Schematic configuration of the TITAN experiment

There are three main components that constitute the TITAN experiment: RFQ, EBIT and MPET (Fig. 3).

**RFQ**

The primary objective of the Radio Frequency Quadrupole (RFQ) is to cool and bunch the continuous, high energy (60KeV) ion beam coming from the ISAC beamlines to match the lower acceptance of the elements along the TITAN beamlines.

Consider an electrode configuration of 2 positive electrodes and 2 negative electrodes (Fig. 4). Initially, a positive ion placed inside this structure will accelerate towards one of the negative electrodes. But before the ion reaches the negative electrode, switch the negative electrodes into positive ones, and vice-versa such that the ion will reverse direction. This periodic, time dependent electric field with alternating polarity traps the ions in 2-D.

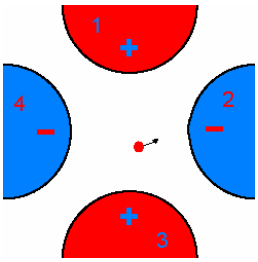

Fig 4 The RFQ's trapping electrodes

Furthermore, the RFQ is segmented such that by applying a higher potential to the outer sections than to the inner one creating a longitudinal potential well to achieve 3-D trapping along the length of the trap. The capture ions can then be pulsed out by switching the potential on the end rods from high to low voltage which delivers the ions in bunches.

Cooling can be achieved while the ions are trapped because the RFQ is filled with a neutral buffer gas. Collisions between the gas molecules and the beam cause the later to dissipate energy until a state of equilibrium is established. Since the buffer gas is neutral and inert, charge exchange with the ions does not occur and the electric field discussed above prevents the beam from inter-dispersion with the gas while it is cooled.

**EBIT**

A common usage for electron beam ion traps (EBIT) is to trap ions for direct spectroscopic experiments. But TITAN's EBIT was designed for charge breeding the short-lived singly charged isotopes from ISAC into highly charged ions (HCIs). As was mentioned previously, the precision of mass measurements is a function of the ion charge state and the statistical uncertainties can be reduced if the ions to be measured are in highly charged states.

Three segmented electrodes form an electrostatic potential well in the axial direction. Radially, the ions are trapped by a magnetic field produced by two superconducting Helmholtz coils, and also the space-charge of the electron beam (Fig. 5). While confined in 3-D, an intense beam of electrons collide with the trapped ions, strips off their atomic electrons thus step-wise ionizing them to the desired charge state.

At full operational capability, the EBIT will use a gun cathode delivering a maximum current of 5A to quickly and efficiently breed most atomic species into He-like configurations. Thus the EBIT is an essential component of TITAN, required for rapid charge breeding prior to mass measurements in the penning trap.

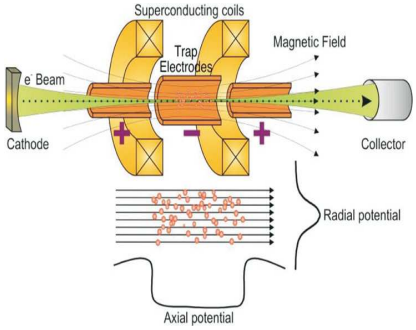

Fig. 5 Trapping Scheme of the EBIT

**MPET**

The penning trap is an indispensable apparatus in mass spectrometry and has been widely used in experiments seeking for the most accurate measurements of isotopic nuclear masses. A Penning trap is a combination of a strong static magnetic field which confines ions in 2-D while a weak electrostatic field keeps the charged particle localized in 3-dimensional space. A configuration of two hyperbolic end cap electrodes coupled with a ring electrode provides a harmonic potential which applies a force on the ions proportional to their distance from the center of the trap (Fig. 6). This mechanism causes them to oscillate with simple harmonic motion. The applied magnetic field triggers the ions to undergo magnetron motion, and the effects of the applied electrostatic field provide the ions with a second reduced cyclotron motion.

Recall that we can determine ion masses if we know the q, B, and cyclotron freq. $\omega_c = qB/2\pi m$. So finally, if we apply a radio frequency (RF) field with resonant frequency equal to the product of the magnetron and cyclotron motions' frequencies, along with time of flight measurements, we can determine the cyclotron frequency and hence be able to determine the mass of the ions.

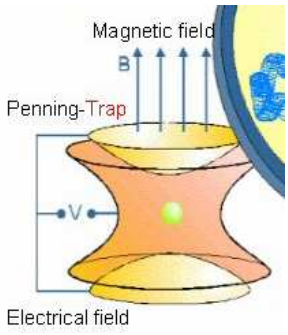

Fig 6 Schematic of the Measurement Penning Trap

# 2 BEAM DIAGNOSTIC SYSTEM

## 2.1 Motivation

The performance of vacuum experiments depends critically on the completeness and quality of their beam diagnostic systems [15]. It is therefore essential to integrate ion beam diagnostic systems into various sections of the TITAN beamlines in order to allow for appropriate online inspection of the ion beam.

Many vacuum systems are designed with tight tolerances on beam loss and emittance blow-up [5]. Thus gaining access to precise and consistent measurements all along the vacuum will permit real-time optimization of the beam position and alignment along the extraction path.

The capabilities of an efficient diagnostic system will aid in proper characterization of the ion beam. Applications include, but are by no means limited to, determining the angular spread of the particles in the beam, quantitative characterization of the beam's spatial intensity distribution, and providing information on other properties and the behaviour of the beams.

Furthermore, a diagnostic system is also good for optimization of operational parameters, alignment of vacuum components, and monitoring beam stability. Thus, a detection and imaging system of high resolution and efficiency is compulsory.

## 2.2 Requirements

Currently many types of detection and imaging systems are in use at various particle accelerator facilities around the world. Many different instruments have been developed for beam diagnostics, and their power has been increased through recent explosion of modern advancements in data acquisition and treatment. Time-honoured techniques include the usage of semi-conductors, gas detectors, secondary emissions, scintillators [5]. But not all systems are suitable or appropriate for use in the design of the TITAN EBIT detector. In particular, several unique requirements must be satisfied.

### 2.2.1 Accommodate Beam from Two Ends

The diagnostic systems we have developed will be located at a junction on the TITAN EBIT beamline. At this location, the general path of a typical ion beam through the TITAN experiment will be such that the incoming beam will injected from the RFQ towards the EBIT and the outgoing beam from the EBIT onwards towards the measurement penning trap upon extraction (Fig. 7). The challenge is that the detector system must be able to accommodate beams whose motion is in opposite directions 180 degrees apart.

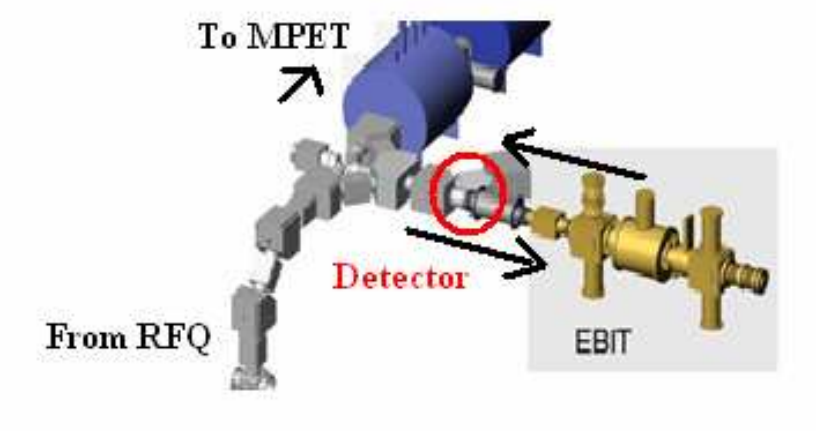


Fig. 7 Detector must accommodate beam from both ends

### 2.2.2 Radiation Damage

The mass-separated, singly charged ions delivered by ISAC into the TITAN beam-lines will be composed of radioactive ion species. Care must taken to avoid direct contact of the beam with the surface of the MCP as the detector is very sensitive to Radiation damage.

There are two main concerns. First, ionizing radiation can break the chemical bonds within a material causing structural damage to the MCP lattice [17]. Second, upon extraction of ions from the EBIT, a large outflow of highly charged ions will be released all at once, magnifying the damaging impact of the radioactive beam [12].

The radiation damage mechanisms the MCP are exposed to include total ionizing dose and displacement damage effects. Charged particles can collide with lead glass atoms and displace them from their lattice sites introducing defects in the material. Any irregularities give rise to a new energetic level and therefore alter the electrical and optical performance of the device [17]. These defects will only degrade the performance of the MCP.

Several scholarly papers have warned against these effects. The drawback of Channel electron Multiplier detectors is their tendency to suffer damage when struck by heavy ions. Therefore signal sizes should be minimised to prolong their life." Also, the Rex-Isolde collaboration has directly mentioned the result of radiation damage to a MCP: "Due to radiation damage, direct implantation of the beam into MCP detectors is limited

only to very low beam intensity applications." [18]. Hence considerations must be taken into the design to prevent direct exposure of the MCP to the radioactive ion beam.

### 2.2.3 Perform high level Diagnostics

The primary usage of our detector system is to perform beam diagnostics. As such, the final image produced must be a good representation of the original ion beam shape. We require a reliable and robust construction that can output a precise image of the position of the ion beam with high spatial resolution and show its corresponding intensity distribution profile. We want to develop a system of high sensitivity, reducing noise as much as possible by implementing proper designs and appropriate shielding. Furthermore, it is desirable that no part of the system should intercept the beam, hence permitting real-time optimization.

### 2.2.4 Limitations

Currently at the prescribe location where the detector will be housed sits an existing standard 8" 6-way cross. Since the entire assembly must fit inside this tight space, the physical restraint to the size of the diagnostic system will call upon some clever designing. Also, recalling that the EBIT relies on a strong magnetic field to trap ions for charge breeding, we must take into consideration how the residual magnetic field of about 20G might influence the mechanism by which the ion beam is detected.

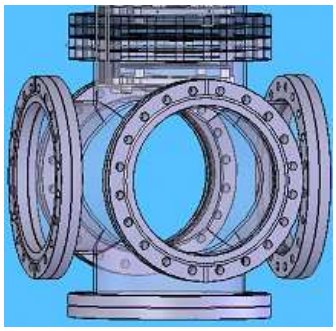

Fig 8 A typical standard 8" 6-way cross

## 2.3 The Daly Detector

### 2.3.1 The original Daly Detector

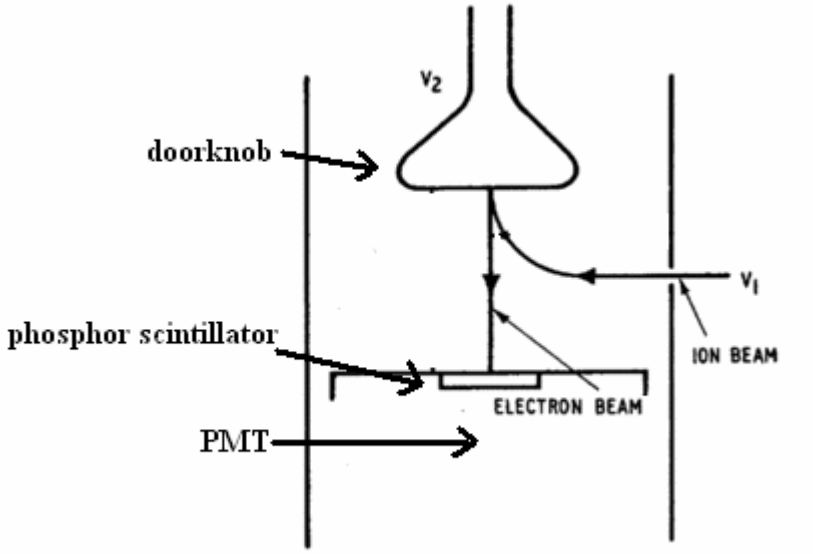


Fig. 9. Schematic diagram of a Daly detector showing the principle of amplification of an incoming positive ion beam.

The original Daly detector, first developed by Norman R. Daly 1960, primarily consists of an overhanging metal "doorknob", a phosphorus scintillator and a photomultiplier (Fig. 9). Prior to its notion, faraday cups were widely used for the purpose of beam detection by measuring the current in a beam of charged particles. However, for ion beams smaller than $10^{13}$ amps, the electrical noise of the Faraday amplifier becomes significant relative to the signal size, so that some form of signal-multiplication becomes necessary. The conception of the Daly detector was the result of this need for a more sensitive detector. [13]

The way the Daly detector works is that as ions pass into the collector region, they are attracted by a large overhanging negative potential applied to the ‘doorknob’. Collision of each ion with the polished electrode surface release secondary electrons. A high voltage usually of 20-40kV between the doorknob and the scintillator accelerates the electrons onto the phosphor screen where they are converted to photons. The resulting light pulse is amplified by a photomultiplier which is situated behind a glass window, exterior to the vacuum system.

Daly detector, often used in molecular beam experiments in combination with time-of-flight mass spectrometry, has several advantages over conventional electron multipliers [13]. The large potential applied to the doorknob ensures approximately 6 secondary electron emissions per ion impact and hence promises a high gain. This leads to excellent signal to noise discrimination. In the analogue mode this system can have a gain about 100 times the Faraday cup. Another significant advantage of the Daly detector is that the photomultiplier tube, the main multiplication electronics in the system can be separated by a window and located outside the main vacuum system. Hence, the gain of the tube is

not affected by changes in the vacuum system and avoids contamination. As such, the Daly detector is robust, with a typical lifetime of several years.

## 2.4 The TITAN EBIT Daly-type design

We have adopted a similar design to the Daly detector, but have made various modifications to suite our purposes as a fully functional diagnostic system. We opted, as much as possible, for a modular design such that system allows for flexibility and variety in use.

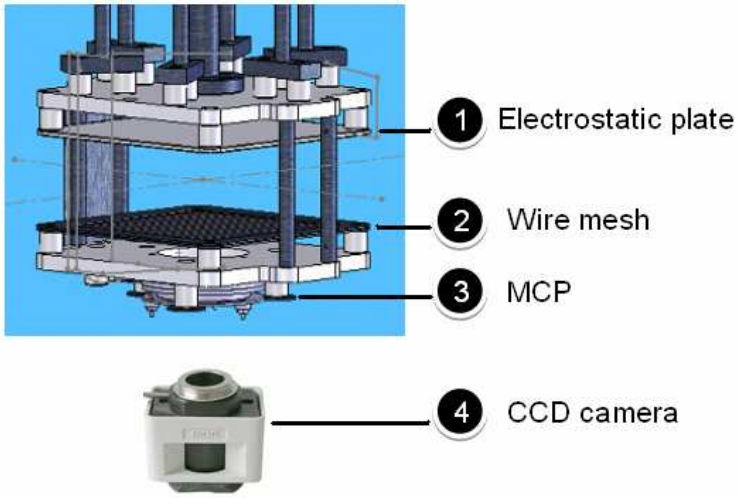


Fig 10 The TITAN EBIT Daly-type detector

### 2.4.1 Basic Components

The design behind TITAN EBIT diagnostic system was motivated by the theme of simple elegance. The structure consisting of only four major components: A high-voltage electrostatic plate, a wire mesh screen, a MCP assembly, and a CCD camera (Fig. 10).

A Micro-channel Plate (MCP) is an array of miniature electron multipliers orientated parallel to one another forming a disc. The plates usually made of material with a low work function such as lead glass, and are treated in such a way as to optimize the secondary emission characteristics of each channel. Usually, a metallic coating of Nichrome is deposited on the front and rear surfaces to serve as input and output electrodes.

Incoming beams of particles impinge upon the front plate of an MCP. Upon striking the channels, electrons are released and which soon turns into a cascade of particles deflecting through the array of tiny channels and accelerates due to the voltage bias between and the first and second plate (Fig 11). A chevron configuration is commonly used to obtain high gain space charge saturated output pulses. Two plates are oriented so that the channel bias angles provide a sufficiently large directional change so as to inhibit positive ions produced at the output of the rear plate from reaching the input of the front

plate. Properly configured, the chevrons typically allow electron multiplication factors of $10^4$-$10^7$ coupled with ultra-high time resolution of 100 ps or less. [19]

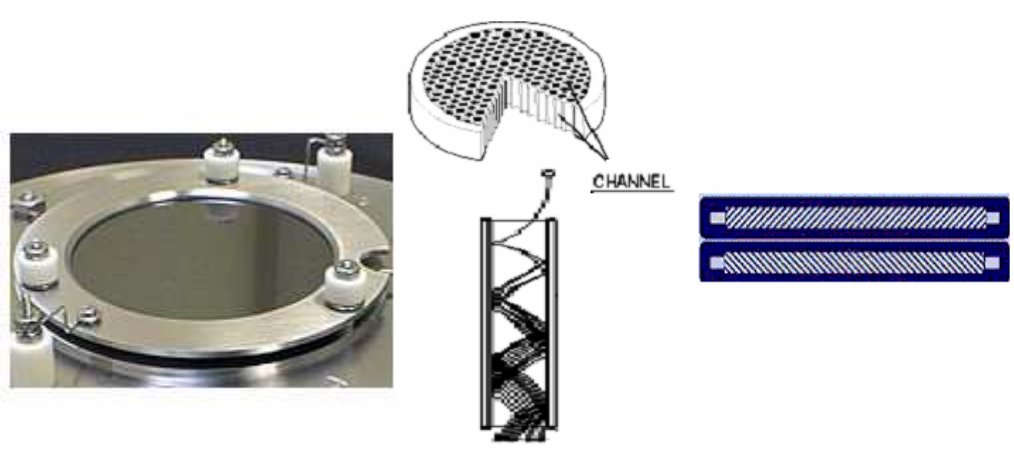


Fig 11 A Microchannel Plate Assembly

In an MCP assembly, an additional phosphor screen is placed at the back of the 2 chevron plates. A fiber optic anode readout provides the phosphor screen user with a two-dimensional image of the output signal coming from the MCPs.

A charge-coupled device (CCD) is a shift registering analog device. Analog signals are transported through successive capacitors using an interline transfer process, where an electronic shutter controls the beginning and end of data taking [2]. When incoming light strikes the surface of the photodiode chips, it is registered as a small electrical charge in each photo sensor. The charges convert to voltage one pixel at a time as they are read from the chip. Additional circuitry in the camera then converts the voltage into digital information. Shift registers send the signal in the photodiodes to make a final image.

Fig 12 CCD camera

### 2.4.2 Principle of Operation

A -5kV potential is placed upon a highly polished aluminium electrostatic plate whose surface is mounted parallel to the direction of beam motion. Positive incoming ions will veer up in attraction to this negative electrode and impinge onto the aluminum plate. As a result, the ions convert into electrons and a secondary electron shower is yielded. The

number of secondary electrons emitted depends on the electronic stopping power of the projectile in the medium. For our case we can expect one electron output for every ion that hits the plate. It is expected that most of the electrons released will have energies of about 1eV at birth. A grid electrode held at ground potential creates a uniform electric field between the plate and the grid that will accelerate the electrons past the bottom grid until they reach the entrance of the MCP detector. The role of the MCP is to amplify the signal of the secondary electrons. An electron multiplying process sends the cascade of electrons onto a phosphor screen where an intensified high resolution image of the beam is produced. The light emissions from the phosphor screen will be observed with a CCD-camera mounted on an optical window outside of the vacuum chamber. The images can then be processed by a standard personal computer with a commercial frame-grabber and displayed directly on the computer monitor. A schematic drawing of the TITAN EBIT beam profiler's principle of operation is shown in fig. 13.

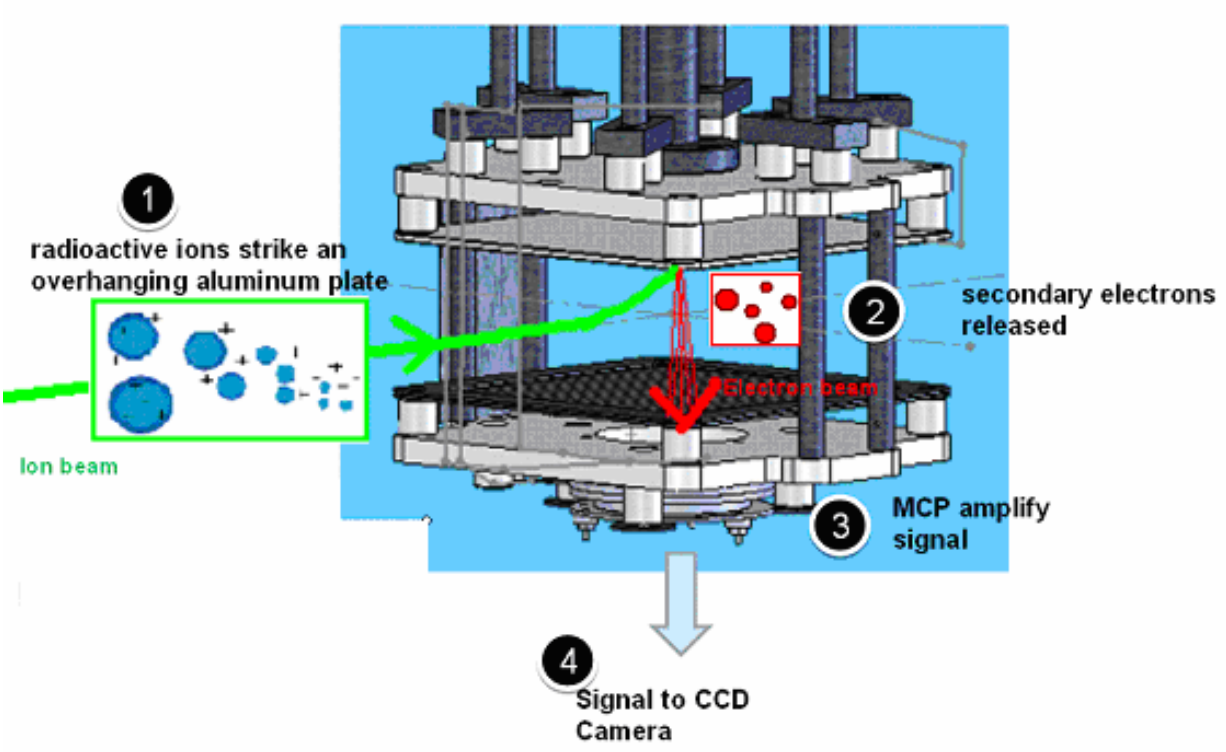


Fig 13 Schematic diagram of the TITAN EBIT beam profiler's principle of operation

The position information of the electrons is preserved since the initial energy of the e- is small. The trajectory of all the secondary electrons will be largely influenced by the same acceleration due to the electric field between the HV plate and the grid [8]. Hence their position on the MCP's entrance plate should reflect the position of impact of the ion beam on the Al plate. Fig. 14 shows the simulated outer edge of the electron beam impinging onto the phosphor screen when we start out with an ideal perfectly circular ion beam. The circular shape indicates that the final image will be a good representation of original beam.

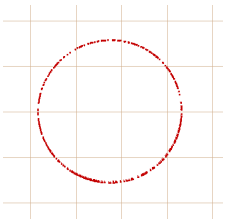

Fig. 14 Red outer ring representing the secondary electrons impinging onto the MCP surface.

The overhanging metal plate is key in our design because it provides a system in which the ions do not strike the MCP multiplier directly. This way, we overcome the problem regarding the detector's sensitivity to radiation damage allowing the equipment to fulfill a long life-time of usage.

| **TITAN EBIT system Specifications:** | |
|---|---|
| **Assembly size:** | |
| HV plate sizes: | 101 x 101mm [square for symmetry] |
| Plate-grid distance | 39.088 mm [confine field] |
| **Applied potentials:** | |
| HV Aluminum plate<br>[2° e- emitted $E_{e^-}$~ 1eV] | V = -5kV |
| Grid electrode [accelerates e- to 5keV.] | V = 0 |
| MCP1 | V = 0 |
| MCP 2 | V = 2kV |
| Phosphor screen. | V = 3kV |

### 2.4.3 Features

**V-on = detection mode:** accepts beam from both ends

The overhanging Daly-type design is so desirable because the system is intrinsically a 2-way beam imaging system. When the -5kV potential to the aluminum plate is switched on and the Daly detector is in detection mode, the ion beam would be diverted from its original trajectory such that it collided with overhanging electrostatic mirror. In fact since the structure is symmetric, the system accepts ion beam from either ends of the system. The mechanism by which the ions veer up towards the Al plate is the same whether they're coming from the RFQ-end or the EBIT-end (Fig. 15a).

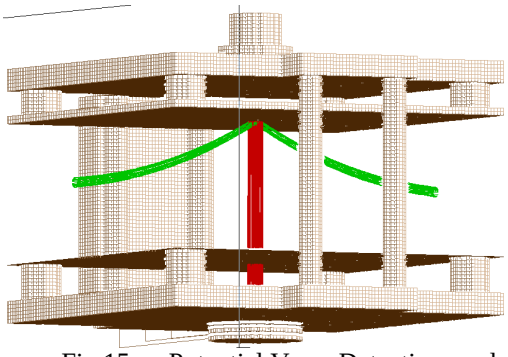

Fig 15a Potential V-on: Detection mode

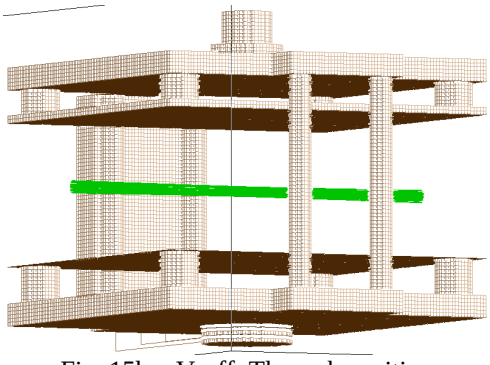

Fig. 15b V-off: Through position

**V-off = Through position:**

When it is desirable to let the ion beam pass through the beamlines, the potential on the electrostatic mirror can be turned off. In the absence of any electric field, the entire structure of the detector essentially becomes invisible to the ions and the beam simply travels straight through. Our design is non-obstructive, and there are no requirements for any rotational or linear pneumatic motion manipulator to deliberately remove the system from the beam path.This is also an advantage as it eliminates the need for frequent alignments every time the system is repositioned (Fig. 15b).

**Faraday cups**

Finally, the tight space inside the 8" 6-way cross is also the housing for a set of faraday cups. As a consequence, although our detector system requires no movement while operational, there might be times when it is desirable to temporarily relocate the detector. We've designed the support structure such that the detector is retractable and hidden well out of the view of the ion beam when it is desirable to accommodate and make use of the Faraday cups (Fig. 16).

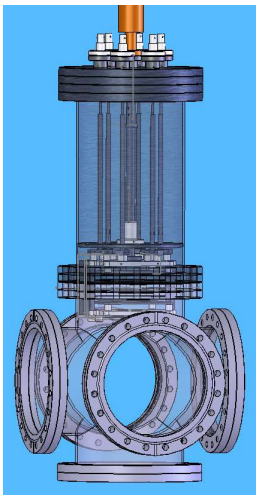

Fig 16 Detector tucked away to allowing Faraday cups to be inserted

# 3 CHALLENGES & CONSIDERATIONS

## 3.1 Structural

### 3.1.1. Electric field shape

The most important consideration of our detector is the shape of the electric field generated between the top electrostatic mirror and the bottom mesh, because it is the interaction of the incoming ions with this field that determines their trajectory as well as the steering of the secondary electrons towards the MCP detector.

We aimed to arrive at a design that was as pragmatic and modular as possible. Different configurations were tested and the final design uses the combination of components that produced the best results. A progression of several preliminary designs can be found in Appendix Bi.

The preference of a square plate was selected such that the ions will see a symmetric field as they approach the detector. For the ions emerging towards the center of the HV plate, they see a electric field approximately like the one generated by an infinitely flat, charged-plane:

$E = \sigma / \varepsilon_o$ where σ = charge per unit area on the plane (SI: C/m 2)

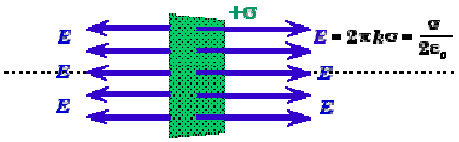


As this equation is independent of distance from the sheet, the E-field is uniform at any distance away from the plane. Hence, the ions far from the fringe fields at the edges will be immersed in an approximately uniform electric field.

Also, the trajectories of ions as they veer upwards towards the high-voltage electrostatic mirror are independent of their charge. This is convenient as the ions extracted from the EBIT will have charge states much higher than those from the RFQ. The ion flight path should be the same because the equations of motion show that as we increase the charge, the energy of the ions also increases. Hence they will move faster and have less time to bend upwards onto the electrostatic mirror.

### 3.1.2. Plate-grid separation

To generate the ideal electric field, we relied on simulations to test out different sizes of HV plates and different plate separation distance between the electrostatic mirror and the grid to determine the optimal parameters needed.

Since this detector design was chosen in order to easily accept ion beams from 2 opposite ends of the detector, we want to make sure that for a beam that is centered with respect to the rest of the elements on the beamline, the ions will hit the center of the detector so that the image on the MCP will thus appear centered regardless of whether the beam arrives from the left or from the right. The EBIT ion injection and extraction energies is planned at 5 keV x q, and the detector's plate and gird separation were determined such the system will perform ideally under this condition.

In the end, it was decided that it is most desirable to have a plate as large as possible to reduce the effects of the fringe fields. However, the physical dimensions were restricted by the size of the 6-way cross housing making the largest size possible, with clearances taken into account, to be 101mm x 101 mm. The optimal plate separation was found using an iterative Interpolation process. Please refer to Appendix Bii.

### 3.1.3 Supporting structure

To stabilize the necessary electrical plates in their respective positions, we need to design a structural support system that would keep them stationary in place. Again, since the shape of the electrical field is so essential to the functionality of the detector, it is compulsory to conjure a structural concept that would minimize distortion to this homogeneous electric field by keeping the rigid support shafts well clear of the strongest parts of the field (Fig.17). Simulations showed that the poles were placed far enough to ensure the ion trajectories will not be compromised.

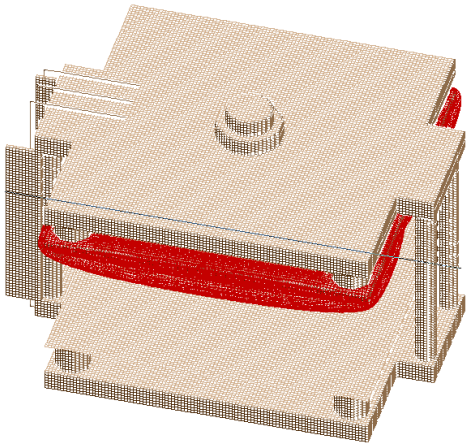

Fig 17. Supporting struts are extended outwards by 2 flaps
so the poles won't cut into the strong E-field.

Furthermore, since we will need a method by which a potential can be delivered to the MCP assembly, wire leads are necessary to connect the bottom plates to the HV feed-throughs at the top. A shield must be employed to screen off the electric field generated by the electrical wire leads. Simulations showed that a c-shaped shield was most efficient in blocking off the field lines. Please refer to Appendix Biii.

## 3.2 Simulations of Environment with Expected Beam Parameters

Appendix A shows the SIMON .gem File used to carry out our simulations.

### 3.2.1 Secondary e- distribution & trajectories

Secondary electrons emitted from aluminum plate are accelerated by a strong and homogeneous electrical field between the HV plate on top and the grid on the bottom. Electrons emitted with different beam energies will have diff angular spread when accelerated from Al plate to MCP. At birth, most of the SE will have an energy of only about 1-3 eV. But in the presence of the strong E field perpendicular to the foil surface, the electrons will immediately accelerate through the 5kV potential difference between the HV plate and the grid. Hence we would expect only a nominal spread in the electron's lateral direction during their passage towards the MCP [18].

Simulations were performed assuming that the secondary electrons are emitted isotropically with no preferred direction from the impacted side of the aluminum plate. But in reality, the emissions are favoured in the direction perpendicular to the surface. Hence, the simulations effectively show the maximum lateral diffusion and give an upper limit of what we can expect (Fig 18).

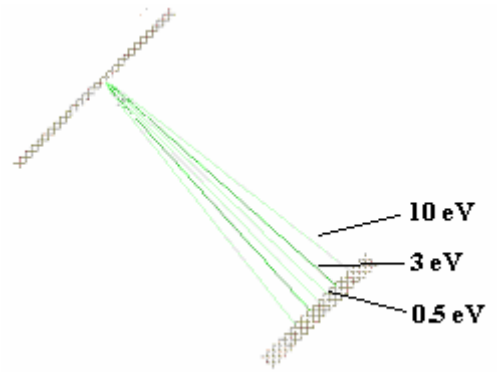


Fig 18 The limits of isotropic emission for $E_{e-}$ = 0.5, 3, 10 eV.
Estimate most will be emitted at ~ 3eV (dark green lines)

### 3.2.2. MCP Efficiency in 5keV range

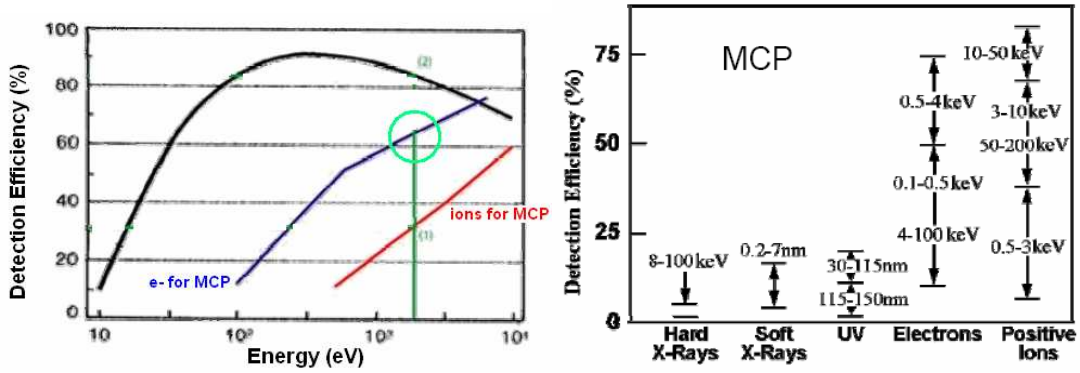


Fig 19. MCP efficiency for several types of particles

It is important to consider the efficiency of the MCP for the type of particles in their particular energy range. Although the secondary electrons initially begin with negligible energy, they will be accelerated up to 5kV by the time they reach the MCP. Thus, we have to consider the performance of the MCP for electrons around 5kV. According to the diagrams [9], the detection efficiency of the MCP for direct electron detection in the 5keV range exceeds 50%. So even if we anticipate only one e- emissions per ion, more than half of the original pulse will still reach the MCP at which point the e- multiplication process will amplify the signal until it is readily readable.

### 3.2.3. Fringe field effects

Because of the fringe field effects at the edges of the high voltage plate, we can not assume that the resultant image will be a good representation when the incoming beam begins its approach far from the center of the beamline. In fact, when Simion simulations were run for a beam forthcoming from the edge of the detector, we see some small but noticeable distortions to the ion image shape (Fig. 20).

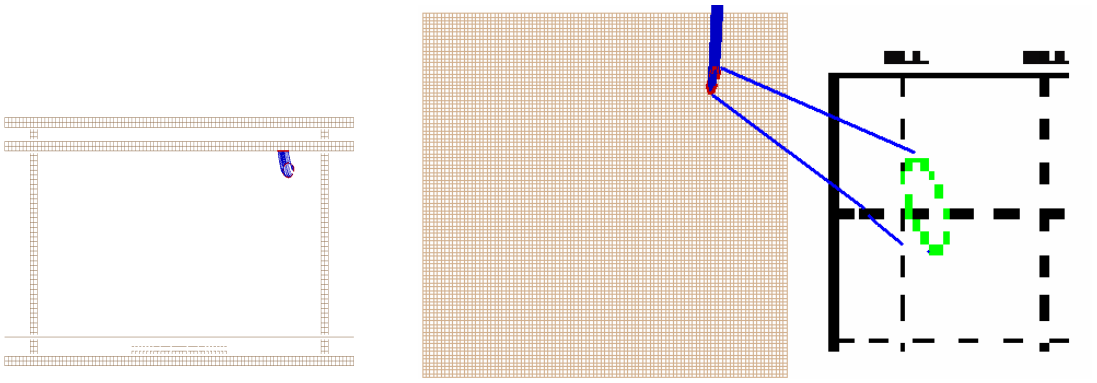

Fig 20 Slight distortion of the beam image upon encountering the edge fringe fields

Fortunately, this should not pose a great deal of a problem since the purpose of our beam profiler is determine proper alignment and telling us precisely when the beam is centered. We can tell immediately from a distorted, off-centered image that the ion beam is in fact not where we want it to be.

When we tweak the alignment such that the beam is centered again, the ions will encounter the homogeneous portion of the electric field, thus restoring the emergent beam shape to be a duplicated mirror image of its original.

### 3.2.4. Ion Beam KE Energy Distribution

One of the main disadvantage of our diagnostic system is that the detector was designed especially to work optimally for a beam with energy of 5keVx q. Although in principle we expect the energy of the ions extracted from the RFQ to hold this value, reality dictates that we're looking more at a energy distribution of around 5000 ± 20eV·q. For example, a beam of $Ne^{10+}$ will have a half width of 200 eV.

Because of this kinetic energy distribution, the ion beam image on the MCP produced by the secondary electrons might be slightly modified. In particular, we expect the beam image seem become elongated along the direction of its motion (Fig 21). Fortunately, simulations show that when ions are initially defined with the expected range of energies, the effects of the distribution does not significantly alter the beam image beyond acceptable limits and the suggested design should fulfill its expected requirements.

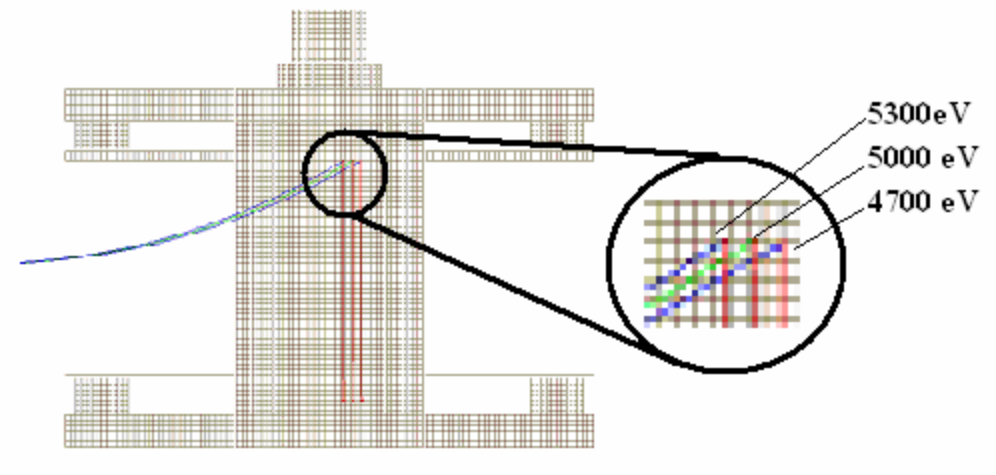


Fig 21 Trajectories of ion beams with energies of 5000 ± 300eV

### 3.2.5. EBIT Magnetic field influence

The trapping scheme of the EBIT requires that there be a 5T magnet in close proximity to the location where the detector will be housed. Since the magnetic field strength will have a $1/r^2$ dependence on the radial distance away from the EBIT magnets, the further away the detector is, the less likely the ion beam will interact with this residual field.

From simulations, the short-coming imposed by presence of the EBIT magnetic field is that the ion beam image produced by the secondary electrons is shifted by a few mm in the direction of travel. Although the beam image is displaced off center, fortunately, the image suffers no deformation in term of its shape.

We have simulated the ion beam trajectories for the only 2 possible locations where the detector can go on the EBIT beamline (Fig 22). The estimated magnetic field at the 6-way cross closest to the EBIT is 20 Gauss. And for the location further away the field reduces to approximately 0.5G, that of the earth's background.

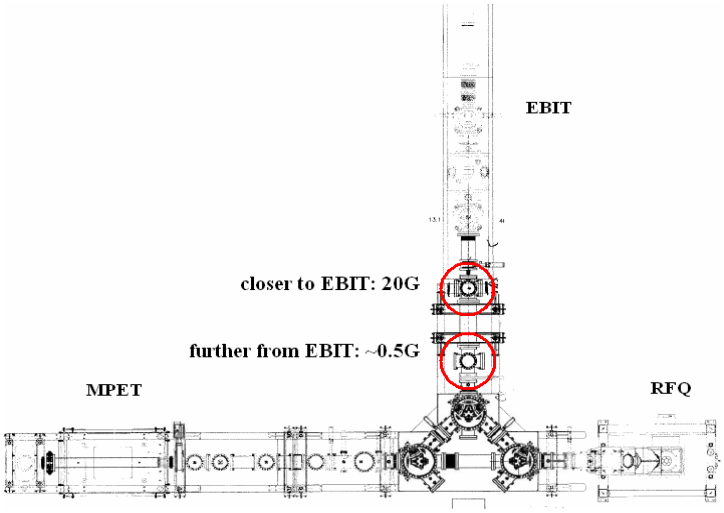


Fig 22 Two possible locations to house the detector

Although the magnetic field is comparatively weaker at the cross furthest from the EBIT, and the improvement to the shift in the ion beam image on the MCP appears to be relatively insignificant. In terms of diagnostic needs, there are advantages in placing our particular detector at location to closest to the magnets and work around the effects of the residual magnetic field as best we can.

# 4 OUTLOOK

## 4.1 Alignment and Calibration

Before the detector becomes operational, special care must be taken to install the system into the vacuum environment and accurately align it with respect to the rest of the components along the beam line. The detector must be calibrated. For this, there are several procedures. It is important to take background measurements and characterize the MCP. We can test the MCP's sensitivity to radiation from various sources so see whether the counting rate is higher for a certain type over another. Such an assessment can test for the response of the system to a possible background of alpha, beta, gamma, or X-ray radiation. Comparing these to the expected signal from the SE shower, we can establish whether the background noise level interfering with our primary signal of interest will be significant [15]. We can also test for the minimum voltage $V_{mcp}$ that needs to be applied to the MCP plate before we observe a signal from the events.

## 4.2 Tests

It is anticipated that the first series of tests performed using the detector will be focused on observing the image of the ion beam, and obtaining its position and intensity profiles to generate a preliminary assessment of the system.

First, comparisons of the actual observed beam shape and those from Simion simulations will be carried out to compare how well the actual conditions were represented by the simulated environment. In particular, the beam trajectory and spot image will be observed under the actual influence of the magnetic and electrostatic fields of the EBIT beamline in the vicinity of the detector. Furthermore, to explicitly prove that the system indeed does not introduce distortion or magnification in the image as predicted from simulations, we can install a set of collimators in the beam path prior to the detector location and compared the MCP obtained images with the upstream collimator images.

The resolution of the camera images are defined by the resolving power of the CCD camera and the frame-grabber, but the resolution of the image on the phosphor screen is defined by the initial energy of the secondary electrons [4]. Therefore, the position and spatial resolution of detection system can be verified by observing the resulting images, and determining the FWHM of the beam profiles. Profile analysis will indicate how well resolved the beam images will be.

Another test we can do with this system is to inspect the intensity distribution of the ion beams. An extension to this is to test for the flexibility of the detection system to different ion beam intensities and in which range the best response will be acquired. Finally, since the ion beam after the RFQ will be clustered in short bunches, investigation of the time resolution of system may be carried out by obtaining fast timing signals from the MCP detector.

# 5 CONCLUSION

We have developed a simple beam diagnostic system for the TITAN EBIT beamline based on observation of secondary electrons created by the impact of an ion beam onto an aluminum plate. Although the design presented here largely resembles the Daly detector, we've modified its precursor such that our required specifications can be met. In particular, the detector is mounted in a stationary position inside the vacuum accommodating ion beams from 2 opposite directions. Beam can pass straight through when the voltages are turned off with no requirements to move the device in and out of the beam path. The system presented will be tested on its capabilities to perform critical analysis the ion beam parameters. It is expected to carry out appropriate online inspection and characterization of the beam position and spatial intensity distribution. Furthermore, it will be useful alignment purposes along the extraction path.


## Acknowledgments

I gratefully acknowledge the support of Alain Lapierre, and the entire TITAN collaboration, for the time, patience, and encouragement that each member has provided throughout this project. It could never have happened if not for the thoughtful preparations they have planed out much in advance. I believe at one point or another, each have contributed to transforming this detector design from imagination to reality. The advice shared has meant more to me than they can imagine. It was such a pleasure to work with you all. Gosh are they ever correct when they say time flies when you're with good company. Many thanks also goes out to Cam Marshall for coming up with all the technical drawings and the staff at the Machine Shop for putting up with my visits 3 times a day.

Fig 23 The 2-Way Daly-Type Beam Diagnostic System for TITAN EBIT

## References:


[1] Bollen G. et al. '*Mass measurement uncertainty formula*' et al. Nucl. Phys. A 693, 3 (2001)

[2] *Charge-coupled device*. Wikipedia: Wikimedia Foundation, Inc. Last modified: 27 August 2007. <http://en.wikipedia.org/wiki/Charge-coupled_device > August 27, 2007.

[3] Currell, Fred, and Fussmann, Gerd, '*Physics of Electron Beam Ion Traps and Sources*' 2005.

[4] Cuttone, G. et al. '*Low Intensity Beam Diagnostics with Microchannel Plate Detectors*' IEEE 1998.<http://ieeexplore.ieee.org/iel4/6051/16227/00751099.pdf?arnumber=751099>

[5] Finocchiaro, Paolo. '*Low Intensity Ion Beam Diagnostics with Particle Detectors'* DIPAC 97 talk Oct 1997. <http://pfmac.lns.infn.it/people/finocchiaro/download/DIPAC97_talk.pdf> Istituto Nazionale di Fisica Nucleare

[6] Froese, Micael Wayne, 'The TITAN Electron Beam Ion Trap: Assembly, Characterization, and First Tests'. 2006

[7] Gillaspy J. D., '*Highly Charged Ions'* 2001

[8] GV Instruments Aug 2007 http://www.gvinstruments.co.uk/isoprobe5.htm

[9] Herlert, Alexander. '*New detector and in-trap decay mass spectrometry at ISOLTRAP*' autumn 2005.

[10] Kruglov, K., Weissman L., et al, '*A beam diagnostic system for low-intensity radioactive beams*' Sept 1999

[11] Lapierre, Alain & the TITAN collaboration.'*The TITAN EBIT: Status & Research Plans*' July 2007.

[12] Lapierre, Alain. '*The TITAN-EBIT: An Electron Beam Ion Trap as a Charge Breeder of Short-Lived Isotopic Highly Charged Ions'*

[13] Mass Spectrometry: Magnetic Sector Mass Spectrometry- Detectors. <http://www.onafarawayday.com/Radiogenic/Ch2/Ch2-3.htm>

[14] O'Sullivan, Erin. '*Low Energy Beam Emittance Detection for the TITAN Project'*, Sept 2006.

[15] Rovelli, A. '*Low intensity beam diagnostics with particle detectors'*

[16] Samson, James A. and Ederer, David L. '*Vacuum Ultraviolet Spectroscopy*' Academic Press 2000, San Diego, CA

[17] Sirianni, Marco and Mutchler, Max. '*Radiation Damage in HST Detectors*' <http://www-int.stsci.edu/~sirianni/PAPERS/SDW2005_sirianni_radiation.pdf>

[18] Van den Bergh, P. et al. '*The Rex-Isolde Beam Diagnostic System*', CP376 American Institute of Physics, 2001.

[19] Wiza, Joseph Ladislas. '*Microchannel Plate Detectors*' Nuclear Instruments and Methods, Vol. 162, 1979, pg. 587-601.

## **Appendix A:** SIMON .gem File for simulations

```
; Daly Test Configuration- Square, no sides + struts
; Last modified: July 18,07

; Define PA to create
PA_Define(200,200,200,planar,none,e)

Locate(0,0,0,1,0,0,0)
{

; Define electrodes
e(1)                                                    ; 1st MCP
{  Locate(100,62,100,1,0,0,90)
   {  Fill
      {   Within {cylinder(0,0,0,12.7, 12.7,1)}
      }
   }
}

e(2)                                                    ; 2nd MCP
{  Locate(100,61,100,1,0,0,90)
   {  Fill
      {   Within {cylinder(0,0,0,12.7, 12.7,1)}
      }
   }
}

e(3)                                                    ; bottom phosphor screen
{  Locate(100,59,100,1,0,0,90)
   {  Fill
      {   Within {cylinder(0,0,0,12.7, 12.7,1)}
      }
   }
}

e(4)                                                    ; top Al plate
{  Locate(100,121,100,1,0,0,0)                          ; plate bottom @ 120 b/c center box
   {   Fill                                                     & 2mm thick plate !!
      {  Within{centered_box3d(0,0,0,101,2,101)}        ; (101x101mm plate)
      }
   }
}

e(5)                                                    ; top/bottom support plates
{  fill
   {   Locate(100,100,100,1,0,0,0)
      {       within{centered_box3d(0,32,0,101,6, 101)}
              within{centered_box3d(0,-32,0,101,6, 101)}

              locate(0,0,0,1,0,0,90)                    ; bottom hole for MCP assem.
              {         notin {cylinder(0,0,30,14,14,10)}
              }
      }
     Locate(87,71,159,1,0,0,90)                         ; 4 side poles + Tabs ; left posts
```

```
    {   Within {cylinder(0,0,0,3,3,58)}
    }
    Locate(113,71,159,1,0,0,90)
    {   Within {cylinder(0,0,0,3,3,58)}
    }
    Locate(82,129,163,1,0,0,0)
    {   Within {box3d(0,0,0,36, 6,-11)}
    }
    Locate(82,65,163,1,0,0,0)
    {   Within {box3d(0,0,0,36, 6,-11)}
    }
    Locate(87,71,41,1,0,0,90)                          ; right posts
    {   Within {cylinder(0,0,0,3,3,58)}
    }
     Locate(113,71,41,1,0,0,90)
    {   Within {cylinder(0,0,0,3,3,58)}
    }
    Locate(82,129,37,1,0,0,0)
    {   Within {box3d(0,0,0,36, 6,11)}
    }
    Locate(82,65,37,1,0,0,0)
    {   Within {box3d(0,0,0,36, 6,11)}
    }

    Locate(100,100,162,1,0,0,0)                        ; shield
    {   Within {centered_box3d(0,0,0,35,58,1)}
    }
    Locate(118,71,162,1,-90,0,0)                       ; right wing
    {   Within {box3d(0,0,0,10,58,1)}
    }
    Locate(82,71,162,1,90,0,0)                         ; left wing
    {   Within {box3d(0,0,0,-10,58,1)}
    }

    Locate(100,135,100,1,0,0,90)                       ; top actuator post
    {   Within {cylinder(0,0,0,10,10,5)}
    }

    Locate(100,140,100,1,0,0,90)
    {   Within {cylinder(0,0,0,7,7,55)}
    }
  }
}

e(6)                                                   ;  ceramics
{  Fill
  {  Locate(144,122,144,1,0,0,90)                      ; top
    {   Within {cylinder(0,0,0,5,5,10)}
    }
    Locate(56,122,144,1,0,0,90)
    {   Within {cylinder(0,0,0,5,5,10)}
    }
    Locate(144,122,56,1,0,0,90)
    {   Within {cylinder(0,0,0,5,5,10)}
    }
    Locate(56,122,56,1,0,0,90)
```

```
    {   Within {cylinder(0,0,0,5,5,10)}
    }
    Locate(144,71,144,1,0,0,90)                    ; bottom
    {   Within {cylinder(0,0,0,5,5,10)}
    }
    Locate(56,71,144,1,0,0,90)
    {   Within {cylinder(0,0,0,5,5,10)}
    }
    Locate(144,71,56,1,0,0,90)
    {   Within {cylinder(0,0,0,5,5,10)}
    }
    Locate(56,71,56,1,0,0,90)
    {   Within {cylinder(0,0,0,5,5,10)}
    }
  }
}

e(7)                                               ; bottom flat grid
{  Locate(100,81,100,1,0,0,0)
  {   Fill
    {  Within{centered_box3d(0,0,0,101,0.2,101)}   ; 101x101mm grid
    }
  }
}

e(8)
{  Fill
  {  Locate(100,100,198,1,0,0,0)                   ; z-axis tube
    {   Within {cylinder(0,0,0,76,76,196)}
    }
    Locate(198,100,100,1,90,0,0)                   ; x-axis tube
    {   Within {cylinder(0,0,0,76,76,196)}
    }
    Locate(100,198,100,1,0,0,-90)                  ; y-axis tube
    {   Within {cylinder(0,0,0,76,76,196)}
    }
    Locate(100,100,198,1,0,0,0)                    ; z-axis ID
    {   notin {cylinder(0,0,0,74,74,196)}
    }
    Locate(198,100,100,1,90,0,0)                   ; x-axis ID
    {   notin {cylinder(0,0,0,74,74,196)}
    }
    Locate(100,198,100,1,0,0,-90)                  ; y-axis ID
    {   notin {cylinder(0,0,0,74,74,196)}
    }
  }
}

e(9)
{  Fill
  {   Locate(92,63,167,1,0,0,0)                    ; left wire
    {  Within{box3d(0,0,0,0.2,77,0.2)}
    }
    Locate(92,63,167,1,0,0,0)                      ; bottom horz
    {  Within{box3d(0,0,0,0.2,0.2,-54)}
    }
```

```
      Locate(92,140,167,1,0,0,0)
      {  Within{box3d(0,0,0,0.2,0.2,-30)}                    ; top
      }
   }
}

e(10)
{  Fill
  {    Locate(100,62,167,1,0,0,0)                            ; center wire
       {  Within{box3d(0,0,0,0.2,78,0.2)}
       }
       Locate(100,62,167,1,0,0,0)
       {  Within{box3d(0,0,0,0.2,0.2,-54)}
       }
       Locate(100,140,167,1,0,0,0)
       {  Within{box3d(0,0,0,0.2,0.2,-30)}
       }
   }
}

e(11)
{  Fill
   {   Locate(108,60,167,1,0,0,0)                            ; right wire
       {  Within{box3d(0,0,0,0.2,80,0.2)}
       }
       Locate(108,60,167,1,0,0,0)
       {  Within{box3d(0,0,0,0.2,0.2,-54)}
       }
       Locate(108,140,167,1,0,0,0)
       {  Within{box3d(0,0,0,0.2,0.2,-30)}
       }
   }
}
}
```

## **Appendix B:** Structural Considerations

### i: Preliminary Designs:

1. monster

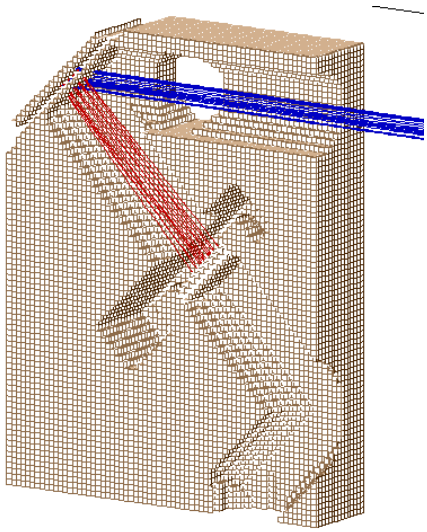

Descripion: Non Daly-type.
Incoming ions hit an aluminum plate that's tilted at 45º and reflected onto an MCP. The signal from the phosphor screen gets reflected by 2 mirrors onto a CCD camera.

Disadvantage: Complicated structure. Existing elements along the beamline must be altered to accommodate this design

2. Box w/ sides

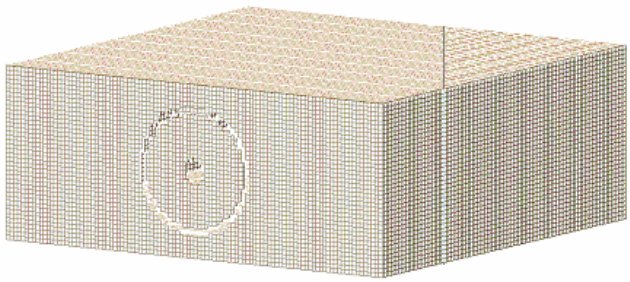

Description: Daly style prototype.
HV plate surrounded by enclosed casing.
Mesh openings on the sides

Disadvantage: Sides restrict the electric field.
Image of a circular ion beam becomes an oval.

3. Circular & Rectangular Plates

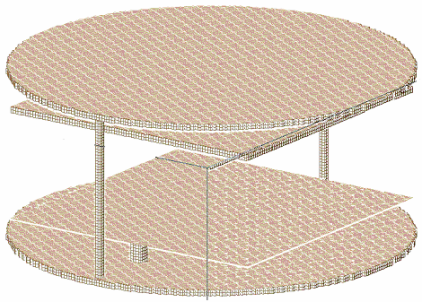

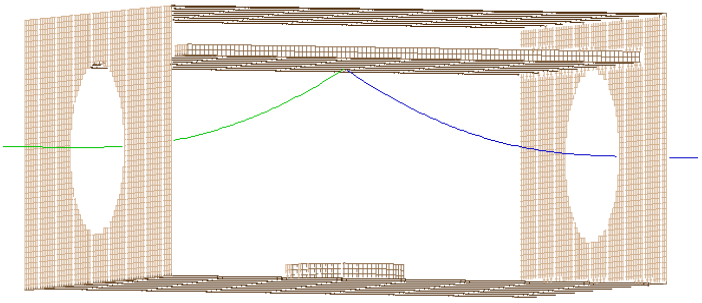

Description: To make best use of the space in the 6-way cross, we considered using circular and rectangular shaped support & potential plates

Disadvantage: non-uniform & non-symmetric fringe fields.
Elongates the beam image

Taking all these preliminary considerations into account, assessment showed that a beam profiling system in the square Daly-type configuration as described in section 3.1.1 will best serve our purposes and usage.

**ii. Ion Images Separation Interpolation to Find Optimal Plate Separation**

Ideally, we want the 2 ion beams from both sides to meet exactly at the center of the detector.

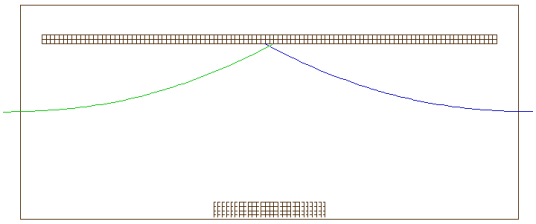

But given the wrong parameters, the 2 beams may never meet half way….

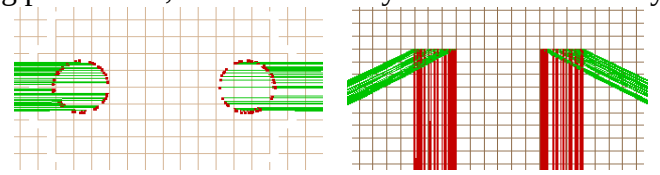

or the beams could overshoot one another and cross over.

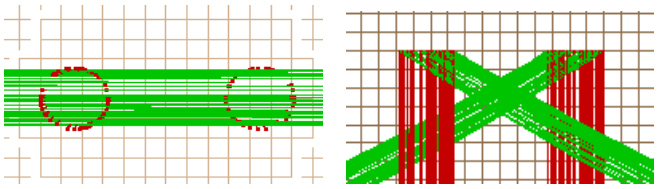

A series of simulations were made and the resulting positions of the 2 beam images on the MCP plate were plotted in their X and Z coordinates. To find the optimal plate separation distance, we seek for the case where the 2 circles to overlap one another.

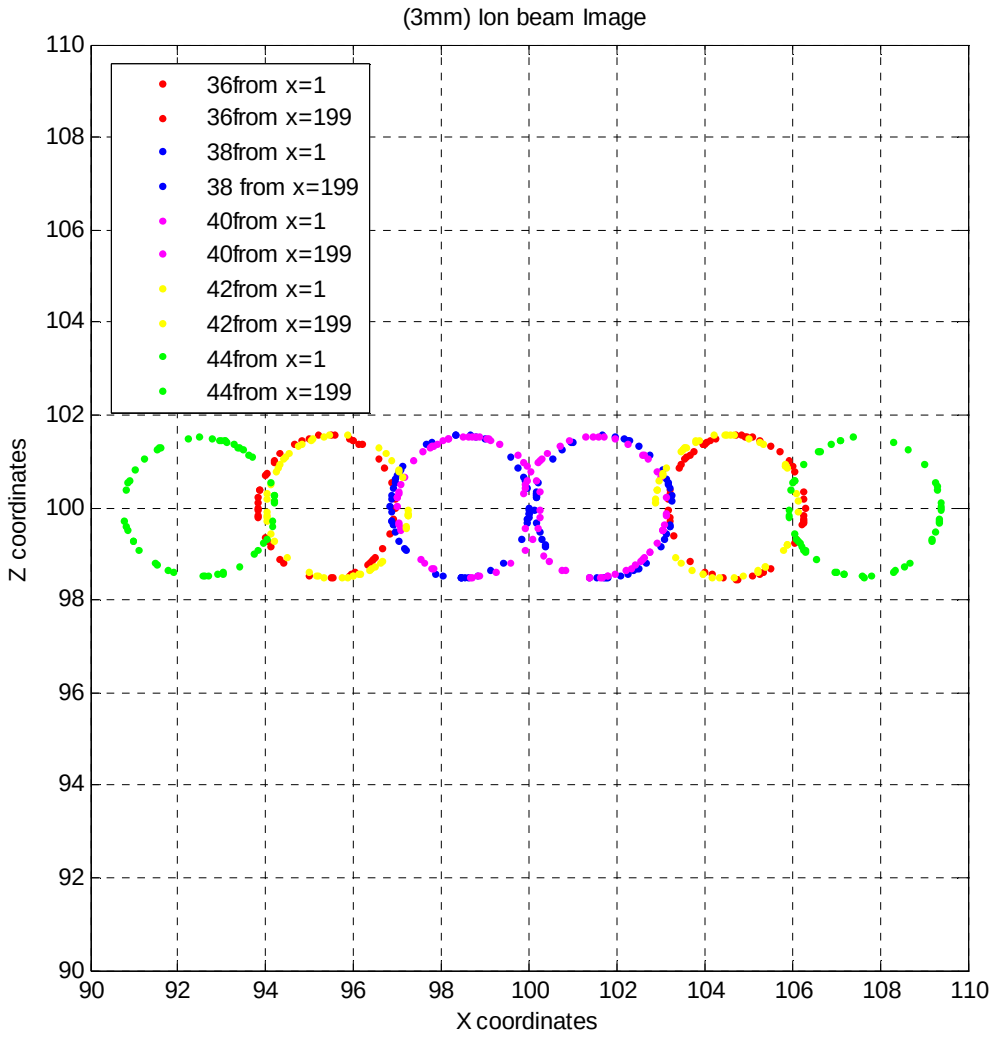

Next, we plotted the separation distance of the 2 beam images as a function of the plate separation distance.

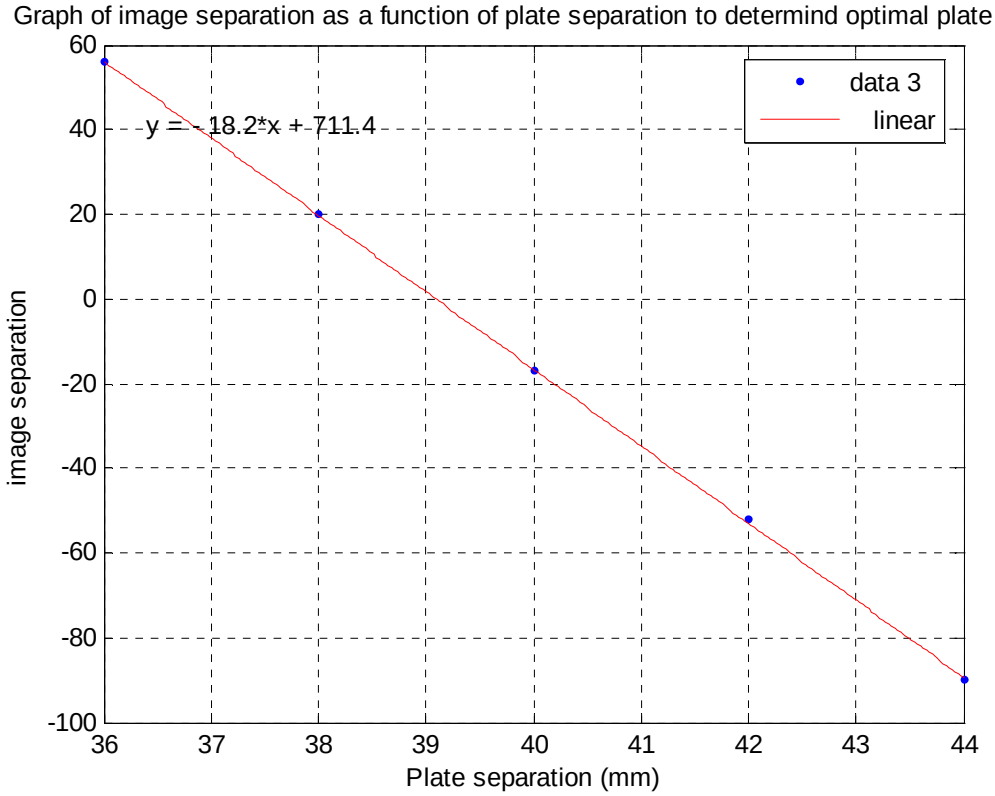


The resulting linear relation satisfied the equation: $y = -18.2x + 711.4$
When the 2 circular images overlap and the image separation distance is zero (y= 0), we find that the HV plate-grid separation distance must be 39.088 mm!!

**iii. Shield Shape**

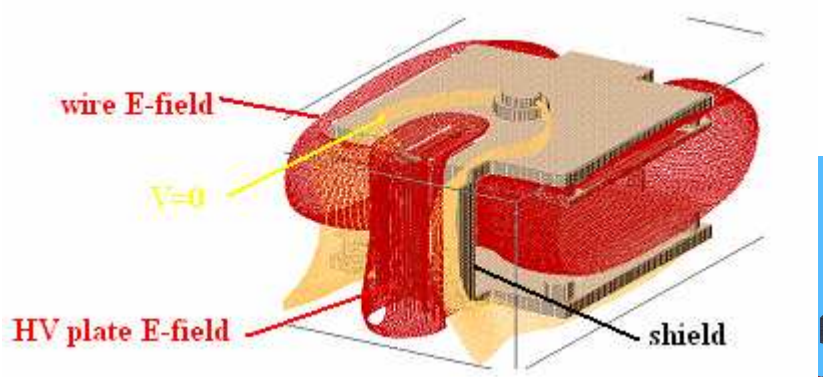


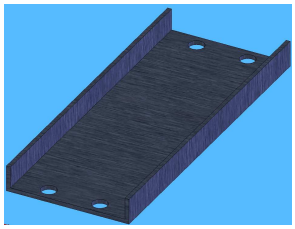

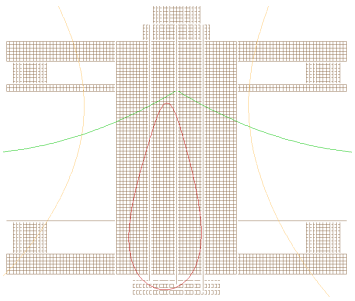

No bends, flat:

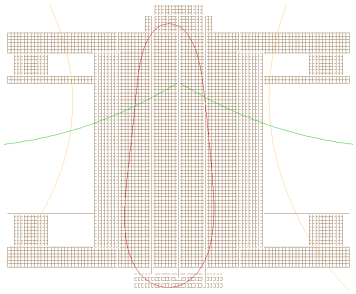

45º bend, wings:

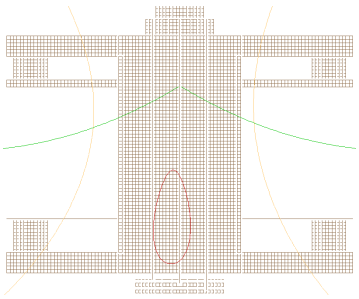

90º bend, c-shaped:

The shield with the 45º bend seems to distort the electric field shape the most. The 45° side plates sticks out and cut off the rounded edge of the HV plate E-field. Contrary, C-shaped shield works best. The strongest field lines (red teardrop in diagram) stays confined to a small area.